PHYSICAL REVIEW B **92**, 041409(R) (2015)

Semiclassical analysis of intraband collective excitations in a two-dimensional electron gas with Dirac spectrum

S. M. Kukhtaruk* and V. A. Kochelap

Department of Theoretical Physics, V.E. Lashkaryov Institute of Semiconductor Physics NASU, Prospekt Nauki 41, Kiev 03028, Ukraine

(Received 26 March 2015; revised manuscript received 3 July 2015; published 24 July 2015)

Solving the initial value problem for semiclassical equations that describe two-dimensional electrons with the Dirac spectrum, we found that collective excitations of the electrons are composed of a few distinct components of the oscillations. There always exist sustained plasma oscillations with the well-known plasmon frequency $\omega_{\rm pl}(k)$. Additionally, there are oscillations with a "carrier frequency" $\omega = v_F k$ slowly decaying in time, according to a power law (v_F and k are the Fermi velocity and wave vector). The reason for the onset of these oscillations has a fundamental character related to the branching of the polarization function of the Dirac electrons. A strongly anisotropic initial disturbance of the electron distribution generates an additional component of the undamped oscillations in the form of an electron unidirectional beam, which are van Kampen's modes in the Dirac plasma.

DOI: 10.1103/PhysRevB.92.041409 PACS number(s): 73.20.Mf, 71.45.−d, 52.35.Fp, 81.05.ue

The polarization properties of electrons determine their response to an external electrical signal, define the collective plasmon and plasmon-phonon modes, as well as many other phenomena involving interactions of the charges. Fundamental and applied aspects of collective excitations in graphenelike systems were discussed in detail in several reviews [1–8]. The polarizability of two-dimensional (2D) electrons with the linear Dirac spectrum $\epsilon(p) = v_F p$ differs considerably from that of the electrons with a parabolic spectrum [$\epsilon(p) \propto p^2$], the latter characteristic for conventional low-dimensional heterostructures. Particularly, the absence of the spectrum curvature leads to less effective screening of the Coulomb potential [1], gives rise to the divergence of the irreducible polarizability [9–11] $\Pi(\omega,k) \propto 1/\sqrt{\omega^2 - v_F^2 k^2}$ at $\omega \to \pm v_F k$, where ω and $\mathbf{k}$ are the frequency and the 2D wave vector, respectively, and v_F is the Fermi velocity. Then, the square-root behavior of the polarizability means that $\Pi(\omega,k)$ is a *double-valued function* on the complex ω plane. For the calculation of the real characteristics of the physical system, the properties of the polarizability as an analytical function on the complex ω plane are critically important. The semiclassical approach based on the analysis of the Boltzmann-Vlasov system of equations allows one to construct the *principal branch* of the polarizability function $\Pi(\omega,k)$ and obtain transparent and easily interpreted results. These results complement those calculated with the use of different quantum mechanical approaches in the long-wavelength limit [9,10].

Recently, new nanoscope techniques were proposed to launch excitations by the sharp tip of an atomic force microscope and to monitor them by a scattering type near-field optical microscope [12,13]. The techniques have enabled the experimental exploration of the spatiotemporal [14–17] and time-resolved [18] dynamics of the collective excitations in graphene and graphenelike systems. Importantly, both the excitation amplitude and phase can be measured [19]. Similar studies have been performed by the use of a resonant antenna plasmon launcher and a near-field optical microscope [20]. Another promising method for plasmon investigation is time-resolved electrical measurements [21,22]. Observed in these works, the macroscopic effects – long-wavelength charge modes and local electric fields – can be described by using the semiclassical approach.

In this Rapid Communication, we present the semiclassical analysis of the *longitudinal intraband* excitations of a 2D electron gas with the Dirac spectrum. It is appropriate to note that the transverse electric mode in graphenelike systems was analyzed in Ref. [23]. We assume an n-doped system and restrict ourselves to excitations with ω and $\mathbf{k}$ for which the interband processes can be neglected at a given electron concentration n and ambient temperature T. Such an approach is valid for $\hbar\omega < \epsilon(p_F)$, $\hbar k < p_F$ at $k_B T \ll \epsilon(p_F)$, with p_F being the Fermi momentum and k_B is the Boltzmann constant (for a detailed discussion, see, for example, Ref. [1]).

The Boltzmann-Vlasov system of equations consists of the collisionless transport equation

$$\frac{\partial F}{\partial t} + v_F \frac{\mathbf{p}}{p}\frac{\partial F}{\partial \mathbf{r}} + e\frac{\partial \Phi}{\partial \mathbf{r}}\bigg|_{z=0}\frac{\partial F}{\partial \mathbf{p}} = 0, \qquad (1)$$

and the Poisson equation

$$\Delta\Phi = \frac{4\pi e\delta[z]}{\kappa}\int \frac{g\, d^2p}{(2\pi\hbar)^2}[F(\mathbf{r},\mathbf{p},t) - F_0(\mathbf{p})]. \qquad (2)$$

Here, the Dirac spectrum is assumed for electrons confined to the sheet at $z = 0$. The electron coordinate and momentum $\mathbf{r},\mathbf{p}$ are the 2D vectors in the x-y plane. $F(\mathbf{r},\mathbf{p},t)$ is the electron distribution function, and $F_0(\mathbf{p})$ is that under equilibrium. $\Phi(\mathbf{r},z,t)$ is the self-consistent electrostatic potential. In Eq. (2), e is the elementary charge, $\delta[z]$ is the Dirac delta function, and g is the degeneracy factor of the electron band (for graphene $g = 4$). The parameter κ depends on the dielectric environment. If the electron sheet is between two materials with the dielectric constants κ_l,κ_h, in the final formulas one shall use $\kappa = (\kappa_l + \kappa_h)/2$.

For the collisionless limit it is necessary to require $\omega\tau \gg 1$, $v_F k\tau \gg 1$, with τ being a characteristic scattering time. For our purposes Eq. (1) shall be linearized. We denote the variation of the distribution function as $\mathcal{F}(\mathbf{r},\mathbf{p},t) \equiv F(\mathbf{r},\mathbf{p},t) - F_0(\mathbf{p})$ and set $\mathcal{F}(\mathbf{r},\mathbf{p},t) = \mathcal{F}_{\mathbf{k}}(\mathbf{p},t)\exp(i\mathbf{kr})$, and $\Phi(\mathbf{r},z,t) =$

*Corresponding author: kukhtaruk@gmail.com

$\Phi_{\mathbf{k}}(z,t)\exp(i\mathbf{kr})$. Now Eqs. (1) and (2) take the form

$$\frac{\partial \mathcal{F}_{\mathbf{k}}}{\partial t} + iv_F\frac{\mathbf{kp}}{p}\mathcal{F}_{\mathbf{k}} = -ie\mathbf{k}\Phi_{\mathbf{k}}(0,t)\frac{\partial F_0}{\partial \mathbf{p}}, \tag{3}$$

$$\frac{d^2\Phi_{\mathbf{k}}}{dz^2} - k^2\Phi_{\mathbf{k}} = \frac{4\pi e\delta[z]}{\kappa}\int\frac{g\,d^2p}{(2\pi\hbar)^2}\mathcal{F}_{\mathbf{k}}(\mathbf{p},t). \tag{4}$$

Following the Landau approach [24], we consider the initial value problem by using the Laplace transform,

$$f_{\omega,\mathbf{k}}(\mathbf{p}) = \int_0^\infty \mathcal{F}_{\mathbf{k}}(\mathbf{p},t)e^{i\omega t}dt,$$
$$\mathcal{F}_{\mathbf{k}}(\mathbf{p},t) = \int_{-\infty+i\sigma}^{\infty+i\sigma} f_{\omega,\mathbf{k}}(\mathbf{p})e^{-i\omega t}\frac{d\omega}{2\pi}, \tag{5}$$

where $\sigma > 0$. Similarly, we define the transformation of the potential, $\phi_{\omega,\mathbf{k}}(z)$. Now, one can easily find the solution for $f_{\omega,\mathbf{k}}(\mathbf{p})$,

$$f_{\omega,\mathbf{k}}(\mathbf{p}) = i\frac{\delta\mathcal{F}_{\mathbf{k}}(\mathbf{p}) - ie\phi_{\omega,\mathbf{k}}(0)\mathbf{k}\,dF_0(\mathbf{p})/d\mathbf{p}}{\omega - v_F(\mathbf{kp})/p}, \tag{6}$$

with $\delta\mathcal{F}_{\mathbf{k}}(\mathbf{p})$ being a given initial perturbation of the electron distribution. The solution to Eq. (4), which decays at $z \to \pm\infty$, also can be easily found. The potential at $z = 0$ is

$$\phi_{\omega,\mathbf{k}}(0) = \frac{-2\pi ie}{\kappa\,k\,\Delta(\omega,k)}\int\frac{g\,d^2p}{(2\pi\hbar)^2}\frac{\delta\mathcal{F}_{\mathbf{k}}(\mathbf{p})}{[\omega - v_F(\mathbf{kp})/p]} \equiv \frac{N(\omega,\mathbf{k})}{\Delta(\omega,k)}, \tag{7}$$

with $\Delta(\omega,k) = 1 - 2\pi e^2\,\Pi(\omega,k)/\kappa k$ and

$$\Pi(\omega,k) \equiv -\int\frac{g\,d^2p}{(2\pi\hbar)^2}\frac{(\mathbf{kp})/p}{[\omega - v_F(\mathbf{kp})/p]}\frac{dF_0(p)}{dp}. \tag{8}$$

It is clear that $\Pi(\omega,k)$ has the meaning of the polarizability obtained in the semiclassical limit. $F_0(\mathbf{p})$ is the Fermi distribution, and then

$$\Pi(\omega,k) = \frac{\kappa\,K}{2\pi e^2}\left[\frac{1}{2\pi}\int_0^{2\pi}d\alpha\frac{\omega}{\omega - v_Fk\cos\alpha} - 1\right], \tag{9}$$

$$K = \frac{e^2gk_BT}{\kappa\hbar^2v_F^2}\ln\left[\exp\left(\frac{E_F}{k_BT} + 1\right)\right], \tag{10}$$

where E_F is the chemical potential.

According to the definition of the Laplace transform (5), in the foregoing Eqs. (6)–(9), $\omega = \omega' + i\omega''$ is the *complex variable* belonging to the upper half plane, $\omega'' > 0$. Under the latter condition, the integral in Eq. (9) can be calculated as

$$\Pi(\omega,k) = \frac{\kappa\,K}{2\pi e^2}\left(\frac{\omega}{\sqrt{\omega^2 - v_F^2k^2}} - 1\right). \tag{11}$$

The function (11) is double valued with two *branch points*, $\omega = \pm v_Fk$, as discussed above.

Consider an analytical continuation of $\Pi(\omega,k)$ given by (9) to the lower half of the ω plane. We start with the use of (11) that is valid for all of the complex ω plane except for the segment at the real axis, $-v_Fk \leqslant \omega' \leqslant v_Fk$. By choosing the cut along this segment, we select the principle branch of the function (11). Defined in such a way, $\Pi(\omega,k)$ is continuous when crossing the real axis at $|\omega| > v_Fk$, while it undergoes a jump in its value at the cut.

As a result of this procedure, we obtain also the function $\Delta(\omega,k)$ as a well-defined function in the complex ω plane. It is easy to see that this function has simple zeros on the real axis,

$$\omega' = \pm\omega_{\mathrm{pl}}, \quad \omega_{\mathrm{pl}}(k) = \frac{v_Fk(1 + k/K)}{\sqrt{(1 + k/K)^2 - 1}}, \tag{12}$$

which are the exact solutions of the equation $\Delta(\omega,k) = 0$. For what follows, it is important that $\omega_{\mathrm{pl}}(k) > v_Fk$.

Before we proceed with a further analysis, let us estimate the value K for the graphene. Assuming a graphene sheet over a SiC substrate ($\kappa_l \approx 9.7, \kappa_h = 1$), setting the electron concentration $n = 2\times10^{12}$ cm^{-2}, and temperature $T = 300$ K, we obtain $E_F \approx 0.16$ eV, $E_F/k_BT \approx 6.12$, $p_F/\hbar \equiv k_F \approx 2.5\times10^6$ cm^{-1}, and $K \approx 3.9\times10^6$ cm^{-1}. That is, $k_F < K$ and for the semiclassical analysis we should use $k < k_F < K$. For example, at $k = 0.05$ K we obtain $\omega_{\mathrm{pl}} \approx 6.4\times10^{13}$ s^{-1} and $v_Fk \approx 2\times10^{13}$ s^{-1}. We refer to this set of parameters as the κ-environment-I. To estimate the criteria of validity of the collisionless approximation, one needs to know the characteristic scattering time τ. The "intrinsic" electron-electron scattering time is of the order of 10^{-11} s [25]. Optical phonon scattering can be neglected for the above accepted parameters. The acoustical phonon scattering time at $T \leqslant 300$ K is estimated to be less than 2×10^{-11} s [2]. Elastic scattering by imperfections is dominant. It can be determined via the phenomenological relationship for the transport time $\tau \approx \mu E_F/ev_F^2$, with μ being the mobility. Assuming $\mu = 2.5\times10^4$ cm^2/V s, we obtain $\tau \approx 4\times10^{-13}$ s and find that the semiclassical approximation criteria are met: $\omega_{\mathrm{pl}}\tau \approx 26 \gg 1$, $v_Fk\tau \approx 8 \gg 1$.

For a graphene sheet in a high-κ environment (for example, graphene in a solvent [26]), the value K can be sufficiently less than k_F. Then the case $k \geqslant K$ may be actual. For example, at $\kappa_l \approx 9.7$, $\kappa_h = 50$, and $k = K$ (κ-environment-II) for the same electron concentration, we obtain $K \approx 7\times10^5$ cm^{-1} and $\omega_{\mathrm{pl}} \approx 8\times10^{13}$ s^{-1}, $v_Fk \approx 7\times10^{13}$ s^{-1} (note that the accepted k is greater than for the κ-environment-I). These estimates show that the excitations considered are rather of the THz diapason.

Now, one can perform the inverse Laplace transform to find desirable functions in the time domain. Below, we will concentrate on the potential at $z = 0$:

$$\Phi_{\mathbf{k}}(t) \equiv \Phi_{\mathbf{k}}(0,t) = \int_{-\infty+i\sigma}^{\infty+i\sigma}\phi_{\omega,\mathbf{k}}(0)e^{-i\omega t}\frac{d\omega}{2\pi}. \tag{13}$$

According to Eq. (7), one can present $\phi_{\omega,\mathbf{k}}(0)$ as a fraction, where the nominator $N(\omega,\mathbf{k})$ is determined by the initial perturbation $\delta\mathcal{F}_{\mathbf{k}}(\mathbf{p})$. First, we will use the typical assumption [24] that the initial perturbation is such that $N(\omega,\mathbf{k})$ has no poles in the ω plane. Then, the analytical properties of both $\Delta(\omega,k)$ and the whole integrand in (13) allow one to deform the integration contour and calculate explicitly the contributions of

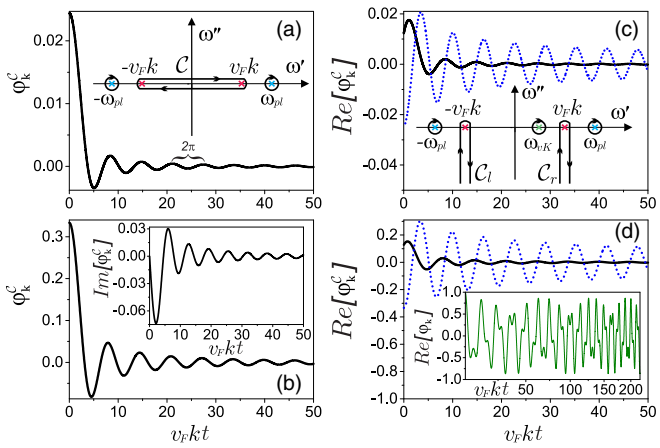

FIG. 1. (Color online) Normalized potential $\varphi^{\mathcal{C}}_{\mathbf{k}}(t)$ for (a), (c) κ-environment-I and (b), (d) κ-environment-II. (a), (b) Isotropic initial perturbation. (c), (d) Strongly anisotropic initial perturbation: solid line, $\alpha_0 = \pi/3$; dotted line, $\alpha_0 = 0$. Insets of (a), (c): Cuts and integral paths on the ω plane. Inset of (b): $\varphi^{\mathcal{C}}_{\mathbf{k}}(t)$ for weak anisotropic perturbation. Inset of (d): Example of temporal pattern for $\omega_{\rm pl} \approx 2\omega_{vK}$.

the residues related to the zeros of $\Delta(\omega,\mathbf{k})$ and branch points:

$$\Phi_{\mathbf{k}}(t) = \Phi^R_{\mathbf{k}}(t) + \Phi^{\mathcal{C}}_{\mathbf{k}}(t), \tag{14}$$

$$\Phi^R_{\mathbf{k}}(t) = -i\frac{\left[\omega^2_{\rm pl} - v_F^2k^2\right]^{3/2}}{v_F^2kK}\{N(\omega_{\rm pl},\mathbf{k})\exp\left[-i\omega_{\rm pl}t\right] - N(-\omega_{\rm pl},\mathbf{k})\exp\left[i\omega_{\rm pl}t\right]\}, \tag{15}$$

$$\Phi^{\mathcal{C}}_{\mathbf{k}}(t) = \oint_{\mathcal{C}} \phi_{\omega,\mathbf{k}}(0)e^{-i\omega t}\frac{d\omega}{2\pi}. \tag{16}$$

In the integral (16), contour $\mathcal{C}$ encloses the cut, as shown in the inset of Fig. 1(a).

In Eq. (14), the first term oscillating with time describes the undamped plasmons excited by the initial perturbation of the distribution function. The latter specifies only the magnitude of the plasmon excitations, while their frequencies do not depend on the initial perturbation. They are determined by the zeros of $\Delta(\omega,k)$ given by Eq. (12). For $k \ll K$, one obtains "the square root law" [9,10], $\omega_{\rm pl} \approx v_F\sqrt{kK/2}$; in the opposite limit, $\omega_{\rm pl} \to v_Fk$.

The last term in Eq. (14) arises due to the existence of *branch points* in $\Delta(\omega,k)$. For electron systems with regular quadratic energy dispersion, there is *no branching* and such a contribution does not exist. In order to perform integration in Eq. (16) we need to specify the initial perturbations. Let us consider a few examples of different initial perturbations.

First, assume that the initial perturbation is isotropic, $\delta\mathcal{F}_{\mathbf{k}}(\mathbf{p}) = \delta\mathcal{F}_k(p)$, i.e., for perturbed electron gas the average momentum and velocity are zero. Then,

$$N(\omega,k) = \frac{i\Phi^0_k}{\sqrt{\omega^2 - v_F^2k^2}}, \quad \Phi^0_k = -\frac{eg}{\kappa\hbar^2k}\int_0^\infty pdp\,\delta\mathcal{F}_k(p), \tag{17}$$

where the square root should be defined as the principal branch on the ω plane with the above discussed cut. Now, the contribution of the residues to the potential equals

$$\frac{\Phi^R_k(t)}{\Phi^0_k} = \frac{2\left[\omega^2_{\rm pl}(k) - v_F^2k^2\right]}{v_F^2kK}\cos[\omega_{\rm pl}(k)\,t]\,. \tag{18}$$

The contour integral of Eq. (16) can be easily estimated for two limiting cases,

$$\frac{\Phi^{\mathcal{C}}_k(t)}{\Phi^0_k} \approx \begin{cases} \frac{k}{K}J_1(v_Fkt)/v_Fkt, & k \ll K, \\ J_0(v_Fkt), & k \gg K, \end{cases} \tag{19}$$

where $J_0(x), J_1(x)$ are the Bessel functions. At $t \gg 1/(v_Fk)$, both expressions can be further simplified,

$$\frac{\Phi^{\mathcal{C}}_k(t)}{\Phi^0_k} \approx \sqrt{\frac{2}{\pi}}\begin{cases} \frac{k}{K}\frac{\cos[v_Fkt-3\pi/4]}{(v_Fkt)^{3/2}}, & k \ll K, \\ \frac{\cos[v_Fkt-\pi/4]}{(v_Fkt)^{1/2}}, & k \gg K. \end{cases} \tag{20}$$

Thus, the initial isotropic perturbation of the electron distribution generates two different components of the electrostatic potential oscillating in time and space. The first component is, obviously, sustained regular plasmon oscillations, excited by the initial perturbation. The second component corresponds to oscillations with the "carrier" frequency $\omega = v_Fk$. The oscillations decay in time according to a power law. Mathematically, they arise due to the existence of the branch points of the polarization function (9). Recovering the space-dependent factor $\exp[i\mathbf{kr}]$, one can see that the $\Phi^R_{\mathbf{k}}$ and $\Phi^{\mathcal{C}}_{\mathbf{k}}$ components correspond to *standing* waves. The main panels of Figs. 1(a) and 1(b) show the normalized potential $\varphi^{\mathcal{C}}_k(t) = \Phi^{\mathcal{C}}_k/\Phi^0_k$ of these oscillations for the two κ environments discussed above.

Interestingly, the ratio of the magnitudes of the two components depends essentially on the wave vector. Indeed, for $k \ll K$, and $t \to 0$ we obtain the estimate $\varphi^{\mathcal{C}}_k \approx k/2K \ll 1$. From Fig. 1(b) we see that at $k = K$, $\varphi^{\mathcal{C}}_k \approx 0.33$. In the opposite case, $k \gg K$, we obtain $\varphi^{\mathcal{C}}_k \approx 1$. That is, the regular plasmon component is preferable excited by long-wavelength perturbations.

Then, consider an initial perturbation of the weak anisotropic form $\delta\mathcal{F}_{\mathbf{k}}(\mathbf{p}) = \delta\mathcal{F}_k(p)\mathbf{pn}/p$, with $\mathbf{n}$ being a unit vector of a preferential direction. We denote the angle between $\mathbf{n}$ and $\mathbf{k}$ as α_0. For this case, at $t = 0$ the perturbed electron gas receives additional momentum and nonzero velocity, while the electron density is unperturbed. The calculation gives

$$N(\omega,\mathbf{k}) = i\frac{\Phi^0_k\cos\alpha_0}{v_Fk}\left[\frac{\omega}{\sqrt{\omega^2 - v_F^2k^2}} - 1\right], \tag{21}$$

where Φ^0_k is given formally by the second relationship of Eq. (17). Calculating the time-dependent potential $\Phi_{\mathbf{k}}(t)$ with this $N(\omega,\mathbf{k})$ function, one can use the analytical continuation discussed above, as well as Eqs. (14)–(16), and the integration contour shown in the inset of Fig. 1(a). The residue contribution to the potential is

$$\frac{\Phi^R_{\mathbf{k}}(t)}{\Phi^0_k} = -2i\cos\alpha_0\frac{\left[\omega^2_{\rm pl}(k) - v_F^2k^2\right]^{3/2}}{v_F^3kK^2}\sin[\omega_{\rm pl}(k)t]. \tag{22}$$

For the contour integral of Eq. (16), we present the results obtained for two limiting cases:

$$\frac{\Phi^{\mathcal{C}}_{\mathbf{k}}(t)}{\Phi^0_k} \approx i\cos\alpha_0 \begin{cases} \left(\frac{k}{K}\right)^2\left[\frac{J_0[v_F kt]}{v_F kt} - 2\frac{J_1[v_F kt]}{[v_F kt]^2}\right], & k \ll K, \\ J_1(v_F kt), & k \gg K. \end{cases} \tag{23}$$

At $t = 0$, both contributions $\Phi^R_{\mathbf{k}}$ and $\Phi^{\mathcal{C}}_{\mathbf{k}}$ equal zero. At $t \gg 1/v_F k$, we obtain

$$\frac{\Phi^{\mathcal{C}}_{\mathbf{k}}(t)}{\Phi^0_k} \approx i\sqrt{\frac{2}{\pi}}\cos\alpha_0 \begin{cases} \left(\frac{k}{K}\right)^2 \frac{\cos[v_F kt - \pi/4]}{(v_F kt)^{3/2}}, & k \ll K, \\ \frac{\cos[v_F kt - 3\pi/4]}{(v_F kt)^{1/2}}, & k \gg K. \end{cases} \tag{24}$$

Thus, weak anisotropic initial perturbation also produces two component oscillations with purely imaginary magnitudes, $\Phi^R_{\mathbf{k}}$ and $\Phi^{\mathcal{C}}_{\mathbf{k}}$, with frequencies $\omega = \omega_{\rm pl}(k)$ and $\omega = v_F k$, respectively. The latter are decaying in time. At small $t \approx 1/v_F k$, these oscillations are quite different from those discussed above, since such a perturbation does not generate directly a space charge and an electrostatic potential. Both are developing with time. The normalized potential $\varphi^{\mathcal{C}}_{\mathbf{k}}(t) = \Phi^{\mathcal{C}}_{\mathbf{k}}/\Phi^0_k$ of these oscillations is illustrated in the inset of Fig. 1(b). The oscillations' magnitude depends on the angle α_0. The magnitude reaches maxima for $\alpha_0 = 0,\pi$. If $\alpha = \pi/2$, the perturbation does not excite the oscillations.

Finally, consider the extremely anisotropic initial perturbation, $\delta\mathcal{F}_{\mathbf{k}}(\mathbf{p}) = 2\pi\,\delta\mathcal{F}_k(p)\,\delta[\alpha - \alpha_0]$, where α is the angle between $\mathbf{p}$ and $\mathbf{k}$, and α_0 determines the anisotropy direction. For the function $N(\omega,\mathbf{k})$ we obtain

$$N(\omega,\mathbf{k}) = \frac{i\Phi^0_k}{\omega - v_F k\cos\alpha_0}, \tag{25}$$

with Φ^0_k still defined by Eq. (17). The function (25) has a pole at the ω' axis, $\omega = \omega_{vK}(\mathbf{k}) \equiv v_F k\cos\alpha_0$. That implies that the above accepted way of analytical continuation of the function $\Pi(\omega,k)$ is no longer applicable. Instead, one can use two cuts along the semi-infinite lines in the lower part of the ω plane, $\omega = \pm v_F k + i\omega''$, $\omega'' \leqslant 0$, as shown in the inset of Fig. 1(c). Now $\Pi(\omega,k)$ is continuous across the real axis everywhere, excluding the points $\omega = \pm v_F k$, and undergoes jumps at the semi-infinite cuts. The time-dependent total potential (13) consists of four contributions:

$$\Phi_{\mathbf{k}}(t) = \Phi^R_{\mathbf{k}}(t) + \Phi^{\mathcal{C}_l}_{\mathbf{k}}(t) + \Phi^{\mathcal{C}_r}_{\mathbf{k}}(t) + \Phi^{vK}_{\mathbf{k}}(t). \tag{26}$$

In contrast to the previous cases, every contribution has nonzero real and imaginary parts. The term $\Phi^R_{\mathbf{k}}(t)$ is the plasmon contribution determined by Eq. (15), with $N(\omega,\mathbf{k})$ given by (25),

$$\frac{\Phi^R_{\mathbf{k}}(t)}{\Phi^0_k} = \frac{2\left[\omega^2_{\rm pl} - v_F^2 k^2\right]^{3/2}}{v_F^2 kK\left(\omega^2_{pl} - v_F^2 k^2\cos^2\alpha_0\right)} \times\{\omega_{\rm pl}\cos[\omega_{\rm pl}t] - i\,v_F k\cos\alpha_0\sin[\omega_{\rm pl}t]\}. \tag{27}$$

The terms $\Phi^{\mathcal{C}_l}_{\mathbf{k}}(t)$ and $\Phi^{\mathcal{C}_r}_{\mathbf{k}}(t)$ are the contour integrals around the left and right cuts, respectively [see Fig. 1(c)]. The main panels of Figs. 1(c) and (d) display the real parts of the total contribution $\Phi^{\mathcal{C}}_{\mathbf{k}} = \Phi^{\mathcal{C}_l}_{\mathbf{k}} + \Phi^{\mathcal{C}_r}_{\mathbf{k}}$ from the contour integrals. The latter can be found explicitly in the limiting case $t \gg 1/(v_F k\sin^2\alpha_0)$:

$$\frac{\Phi^{\mathcal{C}}_{\mathbf{k}}(t)}{\Phi^0_k} \approx \frac{\sqrt{2/\pi}}{\sin^2\alpha_0} \begin{cases} \frac{k}{K}\{\cos[v_F kt - 3\pi/4] - i\cos\alpha_0 \\ \quad\times\sin[v_F kt - 3\pi/4]\}(v_F kt)^{3/2}, & k \ll K, \\ \frac{K}{k}\{\cos[v_F kt - \pi/4] - i\cos\alpha_0 \\ \quad\times\sin[v_F kt - \pi/4]\}(v_F kt)^{1/2}, & k \gg K. \end{cases} \tag{28}$$

The last term in (26) is generated by the additional pole at $\omega = \omega_{vK}(\mathbf{k})$:

$$\Phi^{vK}_{\mathbf{k}}(t) = \frac{\Phi^0_k\exp[-i\omega_{vK}(\mathbf{k})t]}{1 + K(i\cos\alpha_0/|\sin\alpha_0| + 1)/k}, \tag{29}$$

Thus, the strongly anisotropic initial perturbation produces four components of the oscillations. As in the previous cases, one of these components, $\Phi^R_{\mathbf{k}}(t)$, is the sustained plasmon oscillations. The other two components, $\Phi^{\mathcal{C}_l}_{\mathbf{k}}(t)$ and $\Phi^{\mathcal{C}_r}_{\mathbf{k}}(t)$, are oscillations with a "carrier frequency" $\omega = v_F k$: They have different amplitudes and time dependences at finite t and both are similarly decaying in time. Restoring the space-dependent factor $\exp[i\mathbf{kr}]$, one can see that the $\Phi^R_{\mathbf{k}}$ and $\Phi^{\mathcal{C}}_{\mathbf{k}}$ components correspond to *traveling* waves.

The additional fourth component, $\Phi^{vK}_{\mathbf{k}}(t)$, corresponds to *undamped oscillations* with the frequency $\omega_{vK}(\mathbf{k})$. This wave traveling along the wave vector $\mathbf{k}$ (or in the opposite direction) can be interpreted as a particle beam modulated in time and space and moving with the velocity $v_F\cos\alpha_0$. In the physics of a three-dimensional plasma with a regular dispersion of the electrons, such types of waves, with real ω and k, are known as the van Kampen modes [27,28]. Particularly, van Kampen has shown [27] that a sharply anisotropic initial disturbance of the plasma generates waves among which there is such a monoenergetic modulated wave. To distinguish the solution (29) from the other components of oscillations, we will designate it as *a van Kampen mode*.

At a given k, the van Kampen mode depends on two parameters, Φ^0_k and α_0, which characterize the initial perturbation. When the angle of the anisotropy direction, α_0, changes from $\pi/2$ to 0, the frequency of this mode increases from 0 to $v_F k$. At that, the magnitude of the wave varies from infinity ($\alpha_0 = \pi/2$) to zero ($\alpha_0 \to 0$). In the latter case, when the pole $\omega_{vK} \to v_F k$, the $\Phi^{\mathcal{C}}$ contribution sharply increases, as illustrated by numerical calculations presented in Figs. 1(c) and 1(d). Interestingly, in the Dirac plasma, the modulated electron beam corresponding to the van Kampen mode is composed of *unidirectional* but not necessarily monoenergetic electrons, as is seen from the accepted above form of the initial perturbation of the electron distribution.

Note, the region on the ω-k plane, where the van Kampen modes can be excited, coincides formally with the region for which the quantum theory predicts the existence of electron-hole pairs at low temperature [1,4–10]. As contrasted with such one-particle excitations, the van Kampen modes are collective charge excitations.

At a given $\mathbf{k}$, all of the obtained oscillating components are spatially coherent. Their superposition (26) may demonstrate a complex temporal behavior, for example, a beating effect between the plasmon waves and the van Kampen modes, as shown in the inset of Fig. 1(d). To characterize a complex

temporal signal, it is useful to apply a Fourier analysis. We performed such an analysis for the obtained oscillations (26) and found the amplitude and phase of this signal as functions of the frequency. The amplitude shows very narrow peaks at frequencies of the regular plasmons and the van Kampen modes, while their respective phases behave with sharp jumps, as it is typical near resonance. At the frequency $\omega = v_F k$, corresponding to the $\Phi^{\mathcal{C}}_{\mathbf{k}}(t)$ component of oscillations, the amplitude has a smeared spike, however, the phase appears to have a clear characteristic kink. These features of the amplitude and phase of the collective excitations can be verified by contemporary measurement techniques.

In conclusion, we have used the semiclassical approach to obtain transparent results on the dynamics of collective excitations in a Dirac 2D electron gas. By solving the initial value problem for the system of Boltzmann-Vlasov and Poisson equations with different forms of initial disturbances of the distribution function and charge, we found that collective excitations of the electrons with the Dirac spectrum are composed of a few distinct components of the oscillations. Among these, there are always well-known *sustained plasmon oscillations* with the frequency given by Eq. (12). Also, there exist another type of oscillations with the carrier frequency $\omega = v_F k$; they are of a transient character, decaying in time, according to a power law. Mathematically, the latter component of the oscillations arises due to the branching feature of the polarizability function. Finally, a strongly anisotropic initial disturbance generates another component of undamped oscillations of frequency $\omega = v_F k \cos\alpha_0$, with α_0 being the angle between the wave vector $\mathbf{k}$ and the anisotropy direction. We interpreted these undamped oscillations in the form of an electron unidirectional beam and an attendant electrostatic potential both modulated in time and space, as van Kampen's mode [27] in the plasma of the Dirac electrons.

The results obtained demonstrate that the semiclassical approach is adequate to describe the dynamics of collective excitations of THz spectral diapason in the Dirac electron gas.

This work is partially supported by grant NAS of Ukraine for young scientists.

[1] A. H. Castro Neto, F. Guinea, N. M. R. Peres, K. S. Novoselov, and A. K. Geim, Rev. Mod. Phys. **81**, 109 (2009).
[2] S. Das Sarma, S. Adam, E. H. Hwang, and E. Rossi, Rev. Mod. Phys. **83**, 407 (2011).
[3] A. N. Grigorenko, M. Poliniand, and K. S. Novoselov, Nat. Photonics **6**, 749 (2012).
[4] X. Luo, T. Qiu, W. Lu, and Z. Ni, Mater. Sci. Eng., R **74**, 351 (2013).
[5] D. N. Basov, M. M. Fogler, A. Lanzara, Feng Wang, and Y. Zhang, Rev. Mod. Phys. **86**, 959 (2014).
[6] F. J. Garcia de Abajo, ACS Photonics **1**, 135 (2014).
[7] A. Politano and G. Chiarello, Nanoscale **6**, 10927 (2014).
[8] T. Low and P. Avouris, ACS Nano **8**, 1086 (2014).
[9] B. Wunsch, T. Stauber, F. Sols, and F. Guinea, New J. Phys. **8**, 318 (2006).
[10] E. H. Hwang and S. Das Sarma, Phys. Rev. B **75**, 205418 (2007).
[11] V. Ryzhii, Jpn. J. Appl. Phys. **45**, L923 (2006).
[12] R. Hillenbrand, T. Taubner, and F. Keilmann, Nature (London) **418**, 159 (2002).
[13] A. Huber, N. Ocelic, D. Kazantsev, and R. Hillenbrand, Appl. Phys. Lett. **87**, 081103 (2005).
[14] Z. Fei, G. O. Andreev, W. Bao, L. M. Zhang, A. S. McLeod, C. Wang, M. K. Stewart, Z. Zhao, G. Dominguez, M. Thiemens, M. M. Fogler, M. J. Tauber, A. H. Castro-Neto, C. N. Lau, F. Keilmann, and D. N. Basov, Nano Lett. **11**, 4701 (2011).
[15] J. Chen, M. Badioli, P. Alonso-Gonzalez, S. Thongrattanasiri, F. Huth, J. Osmond, M. Spasenović, A. Centeno, A. Pesquera, P. Godignon, A. Zurutuza Elorza, N. Camara, F. J. García de Abajo, R. Hillenbrand, and F. H. L. Koppens, Nature (London) **487**, 77 (2012).
[16] Z. Fei, A. S. Rodin, G. O. Andreev, W. Bao, A. S. McLeod, M. Wagner, L. M. Zhang, Z. Zhao, M. Thiemens, G. Dominguez, M. M. Fogler, A. H. Castro Neto, C. N. Lau, F. Keilmann, and D. N. Basov, Nature (London) **487**, 82 (2012).
[17] Z. Fei, A. S. Rodin, W. Gannett, S. Dai, W. Regan, M. Wagner, M. K. Kiu, A. S. McLeod, G. Dominguez, M. Thiemens, M. M. Fogler, A. H. Castro-Neto, F. Keilmann, A. Zettl, R. Hillenbrand, M. M. Fogler, and D. N. Basov, Nat. Nanotechnol. **8**, 821 (2013).
[18] M. Wagner, Z. Fei, A. S. McLeod, A. S. Rodin, W. Bao, E. G. Iwinski, Z. Zhao, M. D. Goldflam, M. K. Liu, G. Dominguez, M. Thiemens, M. M. Fogler, A. H. Castro-Neto, C. N. Lau, S. Amarie, F. Keilmann, and D. N. Basov, Nano Lett. **14**, 894 (2014).
[19] J. A. Gerber, S. Berweger, B. T. O'Callahan, and M. B. Raschke, Phys. Rev. Lett. **113**, 055502 (2014).
[20] P. Alonso-Gonzalez, A. Y. Nikitin, F. Golmar, A. Centeno, A. Pesquera, S. Velez, J. Chen, G. Navickaite, F. Koppens, A. Zurutuza, F. Casanova, L. E. Hueso, and R. Hillenbrand, Science **344**, 1369 (2014).
[21] N. Kumada, S. Tanabe, H. Hibino, H. Kamata, M. Hashisaka, K. Muraki, and T. Fujisawa, Nat. Commun. **4**, 1363 (2013).
[22] N. Kumada, R. Dubourget, K. Sasaki, S. Tanabe, H. Hibino, H. Kamata, M. Hashisaka, K. Muraki, and T. Fujisawa, New J. Phys. **16**, 063055 (2014).
[23] S. A. Mikhailov and K. Ziegler, Phys. Rev. Lett. **99**, 016803 (2007).
[24] L. D. Landau, On the vibrations of the electronic plasma, Akad. Nauk SSSR. Zhurnal Eksper. Teoret. Fiz. **16**, 574 (1946) [Acad. Sci. USSR. J. Phys. **10**, 25 (1946)].
[25] A. Principi, G. Vignale, M. Carrega, and M. Polini, Phys. Rev. B **88**, 195405 (2013).
[26] F. Chen, J. Xia, D. K. Ferry, and N. Tao, Nano Lett. **9**, 2571 (2009).
[27] N. G. van Kampen, Physica **21**, 949 (1955).
[28] B. B. Kadomtsev, Sov. Phys. Usp. **11**, 328 (1968).